NANO LETTERS
Letter
pubs.acs.org/NanoLett

Vapor-Phase Atomic Layer Deposition of Co_9S_8 and Its Application for Supercapacitors

Hao Li, Yuanhong Gao, Youdong Shao, Yantao Su, and Xinwei Wang*

School of Advanced Materials, Shenzhen Graduate School, Peking University, Shenzhen 518055, China

Supporting Information

ABSTRACT: Atomic layer deposition (ALD) of cobalt sulfide (Co_9S_8) is reported. The deposition process uses bis(*N,N'*-diisopropylacetamidinato)cobalt(II) and H_2S as the reactants and is able to produce high-quality Co_9S_8 films with an ideal layer-by-layer ALD growth behavior. The Co_9S_8 films can also be conformally deposited into deep narrow trenches with aspect ratio of 10:1, which demonstrates the high promise of this ALD process for conformally coating Co_9S_8 on high-aspect-ratio 3D nanostructures. As Co_9S_8 is a highly promising electrochemical active material for energy devices, we further explore its electrochemical performance by depositing Co_9S_8 on porous nickel foams for supercapacitor electrodes. Benefited from the merits of ALD for making high-quality uniform thin films, the ALD-prepared electrodes exhibit remarkable electrochemical performance, with high specific capacitance, great rate performance, and long-term cyclibility, which highlights the broad and promising applications of this ALD process for energy-related electrochemical devices, as well as for fabricating complex 3D nanodevices in general.

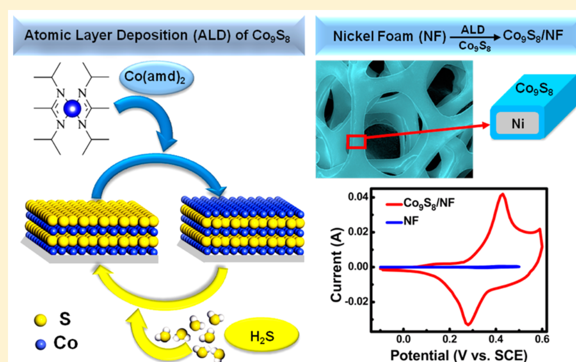

KEYWORDS: *Atomic layer deposition, cobalt sulfide, Co_9S_8, supercapacitor*

Nanostructured transition metal sulfides have recently attracted great attention for applications in energy conversion and storage devices,[1] since many of the transition metal sulfides exhibit highly promising electrocatalytic performance. As a particularly promising material, nanostructured cobalt sulfide (Co_9S_8) has been demonstrated with superb electrochemical performance for a variety of applications in, for instance, supercapacitors,[2,3] lithium-ion batteries,[4] hydrogen evolution reaction,[5] oxygen reduction reaction,[6,7] and dye-sensitized solar cells.[8] For these applications, nanostructuring is particularly important, since it can generally minimize charge transport limitation and shorten the ion diffusion length through the layer of electrochemical active materials, and it can also allow more surface reactive sites to be exposed to electrolyte.[9] Therefore, over the years, great effort has been devoted to develop solution-phase synthetic methods for preparing Co_9S_8 with various nanostructures, such as nanosheets,[10] nanoneedle,[11] nanospheres,[4] yolk–shell structures,[12] as well as in some composite forms with CNTs[13,14] or rGO.[6]

The nanostructuring of active materials may also be achieved by coating the active materials on a 3D structured scaffold by vapor-phase atomic layer deposition (ALD). ALD is a well-known technique for nanoscale device fabrication:[15,16] it takes advantages of saturated, self-limiting surface chemistry reactions and allows one to deposit thin films in a layer-by-layer fashion so that the films can conformally cover any 3D structures with atomic control of the film thickness. With this powerful technique, ideally, one can precisely engineer any surface by coating a conformal thin layer of any active materials without affecting the geometry of the underneath supporting scaffold. This makes ALD particularly useful for fabricating the energy devices which heavily rely on their surface properties (e.g., chemical catalysis,[17,18] electrocatalysis,[19,20] photoelectrochemical catalysis,[21−24] solar cells,[25] and batteries[26−29]), because the engineering of the materials surface properties can be decoupled from the engineering of the geometric structure of the supporting scaffold. On the other hand, ALD can also facilitate many fundamental mechanism studies, since the uniform thin layers of active materials prepared by ALD can minimize many complicated issues, such as inadequate materials dispersion and charge transport limitations, and therefore allow one for pure assessment of the material performance.[30]

Over the past decades, ALD has grown very rapidly with hundreds of different materials have been realized by ALD.[31] But most of the existing ALD processes are for depositing oxides, and, as reviewed recently,[32] only 16 binary sulfides have been realized by ALD so far, missing, unfortunately, many transition metal sulfides that are excellent electrocatalysts, such as cobalt sulfides, iron sulfides, and nickel sulfides. Therefore, the development of new ALD processes for transition metal sulfides is urgently in need.

Received: June 24, 2015
Revised: August 16, 2015

ACS Publications © XXXX American Chemical Society

DOI: 10.1021/acs.nanolett.5b02508
Nano Lett. XXXX, XXX, XXX−XXX

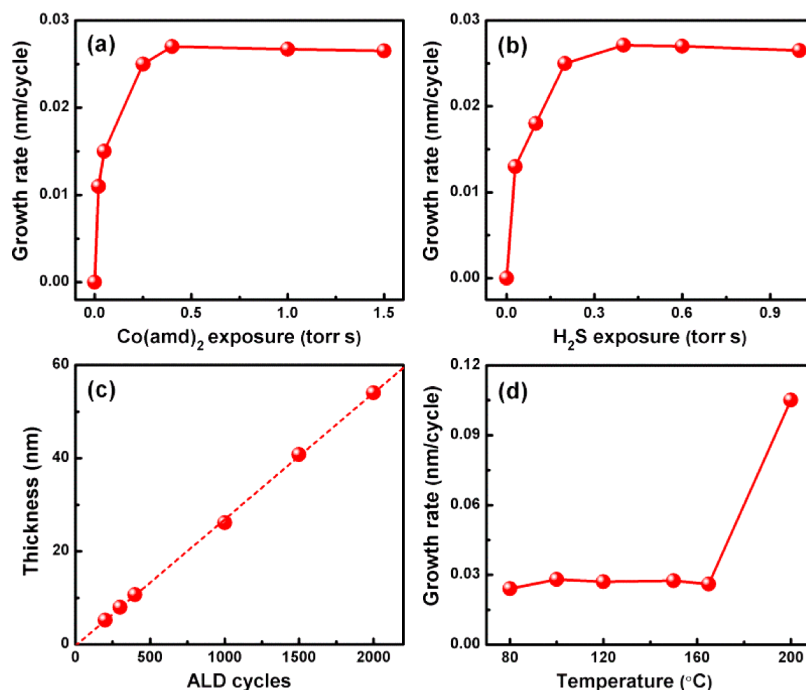

Figure 1. Data plotted in panels a and b showing that the ALD growth rate of Co_9S_8 approaches a constant value (due to saturated, self-limiting surface reaction) as the precursor dosage increases. (a) Growth rate with $Co(amd)_2$ exposure at fixed H_2S exposure of 0.4 Torr s. (b) Growth rate with H_2S exposure at fixed $Co(amd)_2$ exposure of 0.4 Torr s. (c) Film thickness as a function of total ALD cycles. The deposition temperature for a, b, and c were 120 °C. (d) Growth rate as a function of deposition temperature. Saturated exposures of 0.4 Torr s for both $Co(amd)_2$ and H_2S were used for c and d.

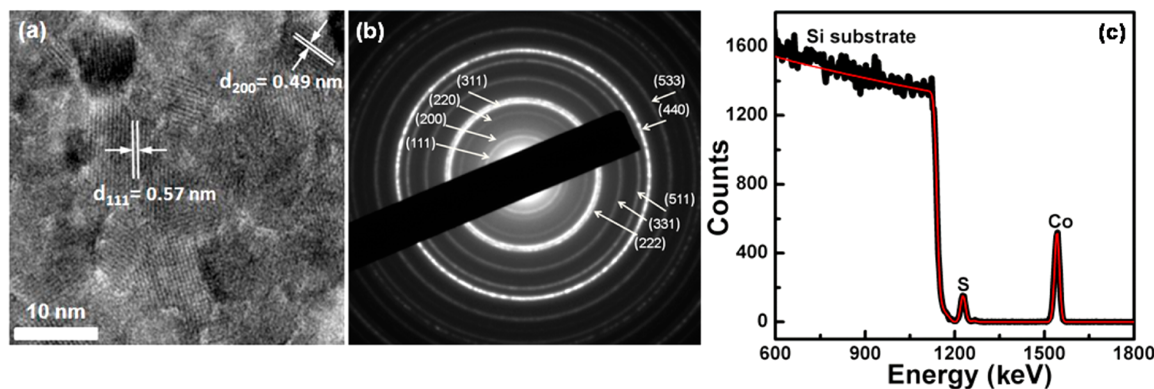

Figure 2. TEM (a) image and (b) electron diffraction pattern of a ~ 10 nm Co_9S_8 film deposited on a SiN_x TEM grid at 120 °C. (c) RBS spectrum (thick black line) of a ~ 8 nm Co_9S_8 film deposited on Si substrate at 120 °C, with simulated spectrum (thin red line) plotted for comparison.

In this Letter, we report an ALD process for Co_9S_8. The process was able to deposit high-quality Co_9S_8 films with an ideal layer-by-layer ALD growth fashion. High-quality Co_9S_8 films could also be conformally deposited into deep narrow trenches with aspect ratio of 10:1, which demonstrates the high promise of this ALD process for fabricating high-aspect-ratio 3D nanodevices. Further, as a demonstration for electrochemical device applications, we employed this ALD process to deposit Co_9S_8 on porous nickel foams as the electrodes for supercapacitors, and, as expected, excellent electrochemical performance was obtained.

Vapor-phase ALD of Co_9S_8 thin films was carried out in a home-built ALD reactor by using bis(*N*,*N*′-diisopropylacetamidinato)cobalt(II) ($Co(amd)_2$) vapor as the cobalt precursor and H_2S (1%) as the coreactant gas. During the deposition, the cobalt precursor was heated to 60 °C, and was delivered into the reactor chamber with the assist of N_2 carrier gas. The deposition temperature was varied from 80 to 200 °C for investigating the film growth behavior. We found that the film growth followed an ideal saturated, self-limiting, layer-by-layer ALD growth fashion at the deposition temperature from 80 to 165 °C. As a typical example, the self-limiting growth behavior at 120 °C is demonstrated in Figure 1a−b. With the variation of the exposure for $Co(amd)_2$ (Figure 1a) or H_2S (Figure 1b), while keeping fixed the exposure for the other, clear saturation behavior for the growth rate was manifested when the exposures for $Co(amd)_2$ and H_2S were both greater than 0.4 Torr s. The saturated growth rate was 0.27 Å/cycle in this case. Therefore, unless otherwise specified, we used the minimum saturated exposures of 0.4 Torr s for both $Co(amd)_2$ and H_2S in the following deposition experiments.

The linear growth behavior was examined by varying the total number of the ALD cycles up to 2000. As shown in Figure 1c, the thickness of the deposited films followed a linear

DOI: 10.1021/acs.nanolett.5b02508
Nano Lett. XXXX, XXX, XXX−XXX

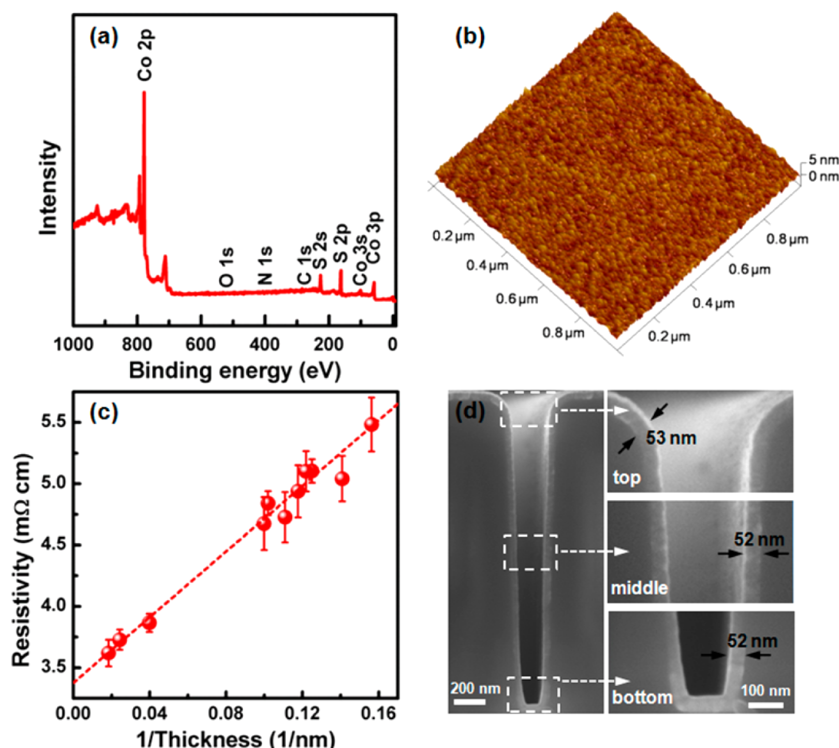

Figure 3. (a) XPS spectrum of a ∼ 25 nm Co_9S_8 film with 45 s Ar^+ sputtering to remove the surface adventitious carbon. (b) AFM image showing an rms roughness of only 0.7 nm for the ∼25 nm Co_9S_8 film. (c) Film resistivity with respect to the reciprocal of film thickness. A linear fit (dash line) with fitted parameters of ρ_0 = 3.4 ± 0.1 mΩ cm and t_0 = 3.9 ± 0.1 nm (see text) is also plotted. (d) Cross-sectional SEM image showing that Co_9S_8 film was conformally deposited (2000 cycles at 120 °C) inside a deep narrow trench with an aspect ratio as high as 10:1.

relation with the total ALD cycles, which suggested that the film thickness could be precisely controlled by digitally varying the total cycle number. The linear fit also showed zero intercept, which indicated that there was no nucleation delay for the deposition and the film started to grow from the first cycle. The growth rate, which was extracted from the slope of the linear fit, was plotted with respect to the deposition temperature as shown in Figure 1d. The growth rate remained almost constant around 0.24−0.28 Å/cycle for the deposition temperature ranging from 80 to 165 °C, which demonstrated a relatively wide temperature window for the ALD process. If the deposition temperature was further raised to 200 °C, a steep increase of the growth rate to 1.05 Å/cycle was observed, suggesting that 200 °C was beyond the temperature window. Therefore, in the following, we only focused our material characterizations on the films deposited within the ALD temperature window.

The microstructure of the deposited Co_9S_8 films was examined by transmission electron microscopy (TEM). Figure 2a−b shows a typical TEM image and the corresponding electron diffraction pattern for a ∼10 nm Co_9S_8 film deposited at 120 °C on a SiN_x membrane grid. The TEM image shows that the film was well-crystallized with the grain size of around 10 nm, and the diffraction ring pattern matched very well with the Co_9S_8 face-centered cubic structure (a = 9.92 Å, JCPDS 86-2273) with no other phases detected. Rutherford backscattering spectrometry (RBS) was performed to determine the Co:S atomic ratios of the deposited films. According to the spectrum shown in Figure 2c, the Co:S atomic ratio was 1.14 ± 0.04, which was in great agreement with a stoichiometric ratio of 1.125 for Co_9S_8.

The purity of the deposited Co_9S_8 films was evaluated by X-ray photoelectron spectroscopy (XPS). The XPS spectrum was collected on a ∼ 25 nm Co_9S_8 film after 45 s of 3 keV Ar^+ sputtering to remove the adventitious carbon on surface. As the spectrum shown in Figure 3a, no carbon (1s, ∼ 284 eV), nitrogen (1s, ∼ 400 eV), or oxygen (1s, ∼ 530 eV) impurity peaks were observed, and only peaks associated with cobalt and sulfur appeared in the spectrum, which indicated that the deposited Co_9S_8 film was quite pure, and the impurity levels of C, N, and O were all below 1 at. % based on our detection limit. Additional high-resolution XPS scans (Figure S1) showed that the spin−orbit split peaks of Co 2p were at 778.3 eV ($2p_{3/2}$) and 793.2 eV ($2p_{1/2}$), and the spin−orbit split peaks of S 2p were at 161.4 eV ($2p_{3/2}$) and 162.5 eV ($2p_{1/2}$), which were all consistent with the reported values for Co_9S_8.[2] The atomic composition determined from the areal intensities of the Co 2p and S 2p peaks were 53 at. % and 47 at. % for Co and S, respectively. Therefore, the Co:S atomic ratio from the XPS results was ∼1.13, which was also consistent with the stoichiometric ratio of 1.125 for Co_9S_8. The surface morphology of the deposited films was examined by atomic force microscopy (AFM). As the AFM image shown in Figure 3b, the film deposited at 120 °C was fairly smooth with an rms roughness of only 0.7 nm for a 25 nm thick film.

As Co_9S_8 is metallic, we also measured the resistivity of the deposited Co_9S_8 films. Generally for thin films with film thickness down to several to tens of nanometers, the transport of electrons can be much influenced by the increased probability of the electron scattering with grain boundaries, interfaces, and surfaces, which can, therefore, appreciably increase the resistivity for thin film materials. To take into account these effects, we employed a simple scattering-induced

DOI: 10.1021/acs.nanolett.5b02508
Nano Lett. XXXX, XXX, XXX−XXX

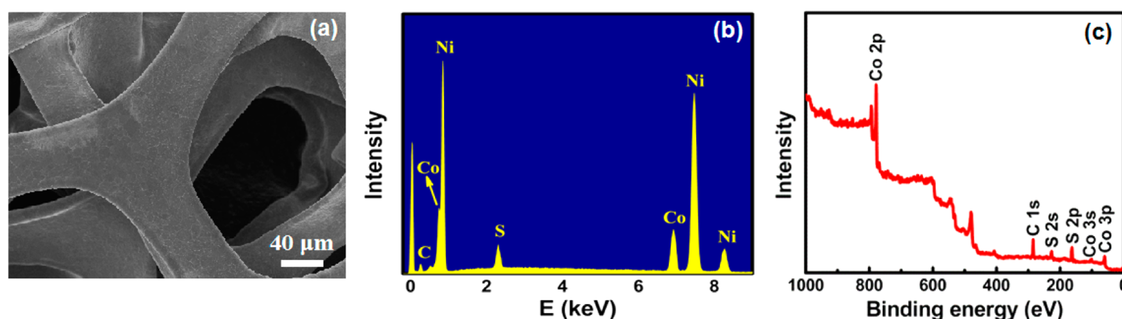

Figure 4. (a) SEM image, (b) EDS spectrum, and (c) XPS spectrum (with Mg Kα X-ray radiation) of Co_9S_8/NF electrode. The Co_9S_8 coating was ~54 nm thick deposited by ALD at 120 °C.

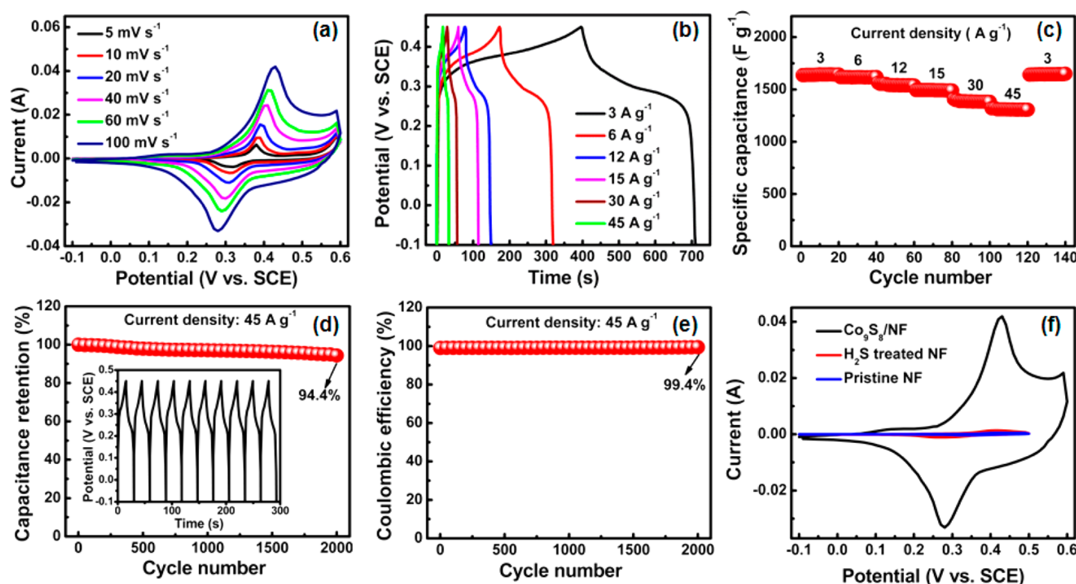

Figure 5. Electrochemical characterizations of Co_9S_8/NF. (a) Cyclic voltammograms at various scan rates. (b) Galvanostatic charge−discharge curves at various current densities. (c) Rate performance with sequentially varying the current density. (d) Long-term cycling performance at a current density of 45 A g^{-1} for 2000 cycles (inset shows the charge−discharge curves for the first 10 cycles). (e) Coulombic efficiency during the above long-term cycling. (f) Comparison of the CV curves for the Co_9S_8/NF electrode, H_2S treated NF electrode and pristine NF electrode (scan rate: 100 mV s^{-1}).

model[33,34] to analyze the thickness dependence of the resistivity. The model states that the thin film resistivity follows a linear relationship with the reciprocal of film thickness, as can be written as $\rho = \rho_0(1 + (t_0/t))$, where ρ is the thin film resistivity, ρ_0 is the bulk resistivity taking into account the scattering effects from impurities, t is the film thickness, and t_0 is the characteristic scattering length, which is associated with the electron mean free path and scattering effects from grain boundaries, interfaces, and surfaces.[33,34] Figure 3c plots the measured resistivity with respect to the reciprocal of film thickness, and the linear fit is also plotted in the same figure. By extrapolating the linear fit to infinitely large thickness, the fitted length t_0 was 3.9 ± 0.1 nm, and the extracted bulk resistivity ρ_0 was 3.4 ± 0.1 mΩ cm, which was in good agreement with the literature value of 3.5 mΩ cm for bulk Co_9S_8 at 300 K.[35]

The step coverage of the deposition was also evaluated. Benefited from the self-limiting surface chemistry of ALD, the Co_9S_8 films were able to be conformally deposited inside deep narrow trenches with high aspect ratios and provided that sufficient exposures of $Co(amd)_2$ and H_2S were supplied.[36] To conformally deposit the Co_9S_8 film inside a 2 μm trench with 10:1 aspect ratio, we increased the exposures of $Co(amd)_2$ and H_2S to 1.5 Torr s and 1.0 Torr s, respectively. As the cross-sectional scanning electron microscopy (SEM) image shown in Figure 3d, the deposited film had a highly uniform thickness throughout the entire trench, which clearly demonstrated the excellent step coverage of our ALD process.

From the above characterizations, we concluded that the Co_9S_8 films deposited by our ALD process were pure and smooth and could be conformally deposited deep narrow trenches, which all suggested that this process is highly promising for coating high-quality Co_9S_8 films on 3D structures for energy-related electrochemical devices. As a demonstration, we further employed this ALD process to deposit Co_9S_8 films on porous nickel foam (NF) substrates and evaluated the electrochemical performance of the prepared Co_9S_8/NF as the electrodes for supercapacitors.

The ALD was performed at 120 °C for 2000 cycles, which produced ~54 nm of conformal Co_9S_8 coating on porous NF to form the Co_9S_8/NF electrode. As the SEM image shown in Figure 4a (see also Figure S2), the deposited Co_9S_8 film was fairly smooth and uniform. Both energy-dispersive X-ray spectroscopy (EDS) (Figure 4b) and XPS (Figure 4c) confirmed the existence of Co and S elements on surface.

DOI: 10.1021/acs.nanolett.5b02508
Nano Lett. XXXX, XXX, XXX−XXX

Also, notice that no appreciable Ni XPS signals (2p, ∼853 eV) were observed in the spectrum. This was because XPS is only sensitive to the top a few nanometer materials, and no appearance of Ni actually suggested an excellent coverage of the Co_9S_8 coating which completely blocked the Ni signals from the underneath NF scaffold.

To evaluate its supercapacitor performance, we conducted careful electrochemical characterizations of the Co_9S_8/NF electrode in a three-electrode cell with 2 M KOH aqueous solution as the electrolyte and platinum foil electrode and saturated calomel electrode (SCE) as the counter electrode and reference electrode, respectively. Series of cyclic voltammetry (CV) measurements were performed with the potential window from −0.1 to 0.6 V with respect to SCE. The scan rate was varied from 5 mV s^{-1} to 100 mV s^{-1}, and the results are shown in Figure 5a. Each of the CV curves showed a well-defined pair of redox peaks, which could be attributed to the following redox reaction of Co_9S_8 in alkaline electrolyte:

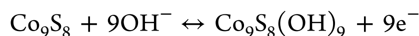

$$Co_9S_8 + 9OH^- \leftrightarrow Co_9S_8(OH)_9 + 9e^-$$

This distinct redox feature suggested that the capacitance was mainly from the Faradaic pseudocapacitance. Also, at a relatively slow scan rate of 5 mV s^{-1}, the anodic and cathodic peaks of the CV curve were located at 0.38 and 0.32 V, respectively, with a voltage difference of only ∼60 mV; even at a high scan rate of 100 mV s^{-1}, the anodic (cathodic) peaks shifted only by 0.04 V upward (downward) to 0.42 V (0.28 V), which suggested that this redox reaction was well reversible and could be used for fast charging/discharging in supercapacitors.

The charging/discharging performance of Co_9S_8/NF was evaluated by the galvanostatic charge−discharge measurements with the potential window of −0.1 to 0.45 V at various current densities ranging from 3 to 45 A g^{-1}. As the results shown in Figure 5b, pronounced plateaus were observed in the charge−discharge process, which again indicated that the capacitance was mainly due to the Faradaic process. Also, the charge−discharge curves were nearly symmetric without any apparent *iR* drop even at a high current density of 45 A g^{-1}, which implied a low polarization of the Co_9S_8/NF electrode. The rate performance was also investigated by sequentially varying the current density from 3 to 6, 12, 15, 30, and 45 A g^{-1}, each of which was tested for 20 charge−discharge cycles, and then followed by 20 cycles of 3 A g^{-1} in the end (Figure 5c). We found that the Co_9S_8/NF electrode was able to deliver excellent specific capacitances of 1645, 1616, 1544, 1493, 1378, and 1309 F g^{-1} at the current densities of 3, 6, 12, 15, 30, and 45 A g^{-1}, respectively. In particular, 80% of the capacitance was still maintained even when the current density was increased by 15 times to 45 A g^{-1}, demonstrating an excellent rate capability of this electrode. This excellent rate capability was no surprise for the ALD-prepared electrodes, since the ALD-prepared active materials were uniform, smooth, and thin, so that the ion diffusion length and the charge transfer length were both minimized. In addition, after the cycling at higher rates, the specific capacitance was managed to return its initial value when the current density returned to 3 A g^{-1}, which indicated a good stability of this Co_9S_8/NF electrode.

Long-term cycling performance was further examined by continuous galvanostatic charge−discharge tests at the current density of 45 A g^{-1} up to 2000 cycles. The results showed that 94.4% of the initial specific capacitance was maintained even after 2000 cycles (Figure 5d), and the Coulombic efficiency was all above 99.4% during the entire cycling (Figure 5e), which demonstrated the remarkable long-term cyclibility of the ALD-prepared Co_9S_8/NF electrodes.

In addition, in order to rule out the possibility of the capacitance contribution from the underneath NF scaffold, we also performed the CV measurements on H_2S treated NF samples and clean NF samples for comparison. As shown in Figure 5f, both of the control samples had negligible capacitance as compared to the Co_9S_8/NF electrode, indicating that the capacitance reported above was entirely from the ALD Co_9S_8 coating layer. As an additional evidence, XPS performed on the H_2S treated NF sample also showed a minimum sulfidation of nickel (Figure S3).

In summary, we reported an ALD process for depositing Co_9S_8 thin films. The process used bis(*N,N′*-diisopropylacetamidinato)cobalt(II) and H_2S as the reactants and showed an ideal ALD layer-by-layer growth fashion for a fairly wide process temperature window from 80 to 165 °C. The deposited Co_9S_8 films exhibited very high film quality with good microstructural crystallinity, stoichiometric composition, high purity, low surface roughness, and good conductivity. Also, the films could also be conformally deposited into deep narrow trenches with an aspect ratio of at least 10:1, suggesting the broad applicability of this ALD process for the conformal coatings of Co_9S_8 on various complex 3D structures. To further demonstrate its electrochemical applications, we prepared the Co_9S_8/nickel foam electrodes by our ALD process for supercapacitors. Benefited from the merits of ALD for making high-quality uniform thin films, the ALD-prepared electrodes exhibited remarkable electrochemical performance, with high specific capacitance, great rate performance, and long-term cyclibility. Therefore, we believe that our ALD process of Co_9S_8 will have broad applications for energy-related electrochemical devices, as well as for fabricating complex nanodevices in general.

Experimental Section. *Atomic Layer Deposition of Co_9S_8 Films.* Co_9S_8 thin films were deposited in a home-built tubular ALD reactor, by using bis(*N,N′*-diisopropylacetamidinato)-cobalt(II) (Co(amd)$_2$) as the cobalt precursor and H_2S as the coreactant gas. The cobalt precursor was kept in a bubbler and heated to 60 °C to provide enough vapor pressure for deposition. The precursor vapor was delivered into the deposition chamber with the assist of purified N_2 gas (through a Gatekeeper inert gas purifier) as the carrier gas. For the coreactant H_2S gas (1% diluted in N_2), it was first delivered into a ∼5 mL gas trap and then delivered into the main deposition chamber for depositing films. The base pressure during purging was ∼0.3 Torr. The deposition temperature was varied from 80 to 200 °C. In order to study the saturation growth behavior, the exposures of Co(amd)$_2$ and H_2S during each ALD cycle were varied by changing the dose number in flow-through mode or changing the exposure time in closed-valve mode. Si wafers were used as the substrates for studying the deposition behavior. Prior to the deposition, the Si substrates were treated with UV/ozone for 5 min.

Co_9S_8 Film Characterizations. The film thickness was determined by X-ray reflectometry (Bruker, D8 Advance). Film microstructure and crystal structure were both examined by TEM (Jeol, JEM-2100). RBS was employed to determine the stoichiometry of the deposited cobalt sulfide films. The RBS experiments were performed in the Heavy Ion Institute at Peking University, using 2.022 MeV helium ions as the incident ions and collecting the backscattered signals at the scattering angle of 165°. XPS (Thermo Scientific, Escalab 250Xi) was

DOI: 10.1021/acs.nanolett.5b02508
Nano Lett. XXXX, XXX, XXX−XXX

used to analyze the chemical composition of the deposited films. Monochromated Al K*α* radiation was normally used for XPS, but since the Co Auger peaks overlap with the Ni 2p peaks, nonmonochromated Mg K*α* radiation from a twin Mg/Al anode was used instead whenever necessary. AFM (Bruker, MultiMode 8) and SEM (Zeiss, SUPRA55) were used to examine the surface morphology and the film conformality, respectively. Sheet resistance was measured by a four-point probe, and resistivity was calculated by multiplying the sheet resistance with the film thickness.

Preparation of Co_9S_8/NF Electrodes. The above ALD process was used to deposit Co_9S_8 film on porous nickel foam (NF) as the electrodes for supercapacitors. Prior to the Co_9S_8 deposition, the as-received NF was sequentially cleaned in dilute hydrochloric acid and deionized water for 10 min of ultrasonication, respectively, and then the cleaned NF was dried at 100 °C in a vacuum oven for 5 h. The ALD of Co_9S_8 was performed at 120 °C for 2000 cycles and produced ~54 nm of conformal Co_9S_8 coating on the NF to form the Co_9S_8/NF electrode. For estimating the per-mass capacitance of the deposited Co_9S_8 as the electrochemical active material for supercapacitors, the total Co_9S_8 mass was determined by dissolving the entire Co_9S_8/NF electrode in HCl:HNO_3 = 3:1 solution and measuring the Co amount by inductively coupled plasma optical emission spectroscopy (ICP-OES, JY2000-2).

Electrochemical Characterizations. Cyclic voltammetry (CV) and galvanostatic charge−discharge experiments were performed on an electrochemical workstation (CHI604E) and a battery test system (Maccor, MC-16), respectively. All of the electrochemical measurements employed a conventional three-electrode cell with 2 M KOH aqueous solution as the electrolyte, and the Co_9S_8/NF electrode, platinum foil electrode, and saturated calomel electrode (SCE) as the working electrode, counter electrode, and reference electrode, respectively.

■ ASSOCIATED CONTENT

Supporting Information

The Supporting Information is available free of charge on the ACS Publications website at DOI: 10.1021/acs.nanolett.5b02508.

Additional high-resolution XPS spectra and high-magnification SEM images (PDF)

■ AUTHOR INFORMATION

Corresponding Author

*E-mail: wangxw@pkusz.edu.cn.

Author Contributions

H.L. and Y.G. contributed equally.

Notes

The authors declare no competing financial interest. During the peer-reviewing process of this paper, a similar ALD process for cobalt sulfide was reported by Peters et al. *ACS Nano* **2015**, *9* (8), 8484−8490.

■ ACKNOWLEDGMENTS

This work was financially supported by NSFC (Grant Nos. 51302007 and 11404011), Guangdong Innovation Team Project (No. 2013N080), and Shenzhen Science and Technology Research Grant (JCYJ20140417144423201). The authors would like to thank Professor Jianming Xue at Peking University for the help of RBS measurement. X. W. would like to thank Professor Jing Kong at Massachusetts Institute of Technology and Professor Roy G. Gordon at Harvard University for valuable discussions.

■ REFERENCES

(1) Gao, M. R.; Xu, Y. F.; Jiang, J.; Yu, S. H. *Chem. Soc. Rev.* **2013**, *42* (7), 2986−3017.

(2) Xu, J.; Wang, Q.; Wang, X.; Xiang, Q.; Liang, B.; Chen, D.; Shen, G. *ACS Nano* **2013**, *7* (6), 5453−5462.

(3) Rakhi, R. B.; Alhebshi, N. A.; Anjum, D. H.; Alshareef, H. N. *J. Mater. Chem. A* **2014**, *2* (38), 16190−16198.

(4) Zhou, Y.; Yan, D.; Xu, H.; Feng, J.; Jiang, X.; Yue, J.; Yang, J.; Qian, Y. *Nano Energy* **2015**, *12*, 528−537.

(5) Feng, L. L.; Li, G. D.; Liu, Y.; Wu, Y.; Chen, H.; Wang, Y.; Zou, Y. C.; Wang, D.; Zou, X. *ACS Appl. Mater. Interfaces* **2015**, *7* (1), 980−8.

(6) Ganesan, P.; Prabu, M.; Sanetuntikul, J.; Shanmugam, S. *ACS Catal.* **2015**, *5* (6), 3625−3637.

(7) Sidik, R. A.; Anderson, A. B. *J. Phys. Chem. B* **2006**, *110* (2), 936−941.

(8) Chang, S.-H.; Lu, M.-D.; Tung, Y.-L.; Tuan, H.-Y. *ACS Nano* **2013**, *7* (10), 9443−9451.

(9) Rui, X.; Tan, H.; Yan, Q. *Nanoscale* **2014**, *6* (17), 9889−9924.

(10) Zhang, X.; Liu, Q.; Meng, L.; Wang, H.; Bi, W.; Peng, Y.; Yao, T.; Wei, S.; Xie, Y. *ACS Nano* **2013**, *7* (2), 1682−1688.

(11) Chen, C.; Ye, M.; Zhang, N.; Wen, X.; Zheng, D.; Lin, C. *J. Mater. Chem. A* **2015**, *3* (12), 6311−6314.

(12) Ko, Y. N.; Choi, S. H.; Park, S. B.; Kang, Y. C. *Chem. - Asian J.* **2014**, *9* (2), 572−576.

(13) Zhou, Y.; Yan, D.; Xu, H.; Liu, S.; Yang, J.; Qian, Y. *Nanoscale* **2015**, *7* (8), 3520−5.

(14) Su, Q.; Du, G.; Zhang, J.; Zhong, Y.; Xu, B.; Yang, Y.; Neupane, S.; Li, W. *ACS Nano* **2014**, *8* (4), 3620−3627.

(15) George, S. M. *Chem. Rev.* **2010**, *110* (1), 111−131.

(16) Johnson, R. W.; Hultqvist, A.; Bent, S. F. *Mater. Today* **2014**, *17* (5), 236−246.

(17) Canlas, C. P.; Lu, J.; Ray, N. A.; Grosso-Giordano, N. A.; Lee, S.; Elam, J. W.; Winans, R. E.; Van Duyne, R. P.; Stair, P. C.; Notestein, J. M. *Nat. Chem.* **2012**, *4* (12), 1030−1036.

(18) Lu, J.; Fu, B.; Kung, M. C.; Xiao, G.; Elam, J. W.; Kung, H. H.; Stair, P. C. *Science* **2012**, *335* (6073), 1205−8.

(19) Viswanathan, V.; Pickrahn, K. L.; Luntz, A. C.; Bent, S. F.; Norskov, J. K. *Nano Lett.* **2014**, *14* (10), 5853−5857.

(20) Wang, H.; Lu, Z.; Xu, S.; Kong, D.; Cha, J. J.; Zheng, G.; Hsu, P. C.; Yan, K.; Bradshaw, D.; Prinz, F. B.; Cui, Y. *Proc. Natl. Acad. Sci. U. S. A.* **2013**, *110* (49), 19701−6.

(21) Dasgupta, N. P.; Liu, C.; Andrews, S.; Prinz, F. B.; Yang, P. *J. Am. Chem. Soc.* **2013**, *135* (35), 12932−5.

(22) Paracchino, A.; Laporte, V.; Sivula, K.; Grätzel, M.; Thimsen, E. *Nat. Mater.* **2011**, *10* (6), 456−461.

(23) Zhong, M.; Hisatomi, T.; Kuang, Y.; Zhao, J.; Liu, M.; Iwase, A.; Jia, Q.; Nishiyama, H.; Minegishi, T.; Nakabayashi, M.; Shibata, N.; Niishiro, R.; Katayama, C.; Shibano, H.; Katayama, M.; Kudo, A.; Yamada, T.; Domen, K. *J. Am. Chem. Soc.* **2015**, *137* (15), 5053−60.

(24) Mayer, M. T.; Du, C.; Wang, D. *J. Am. Chem. Soc.* **2012**, *134* (30), 12406−12409.

(25) Savin, H.; Repo, P.; von Gastrow, G.; Ortega, P.; Calle, E.; Garín, M.; Alcubilla, R. *Nat. Nanotechnol.* **2015**, *10*, 624−628.

(26) Guan, C.; Wang, X.; Zhang, Q.; Fan, Z.; Zhang, H.; Fan, H. J. *Nano Lett.* **2014**, *14* (8), 4852−8.

(27) Han, X.; Liu, Y.; Jia, Z.; Chen, Y. C.; Wan, J.; Weadock, N.; Gaskell, K. J.; Li, T.; Hu, L. *Nano Lett.* **2014**, *14* (1), 139−47.

(28) Scott, I. D.; Jung, Y. S.; Cavanagh, A. S.; Yan, Y.; Dillon, A. C.; George, S. M.; Lee, S. H. *Nano Lett.* **2011**, *11* (2), 414−8.

(29) Meng, X.; He, K.; Su, D.; Zhang, X.; Sun, C.; Ren, Y.; Wang, H.-H.; Weng, W.; Trahey, L.; Canlas, C. P.; Elam, J. W. *Adv. Funct. Mater.* **2014**, *24* (34), 5435−5442.

DOI: 10.1021/acs.nanolett.5b02508
Nano Lett. XXXX, XXX, XXX−XXX

(30) Pickrahn, K. L.; Garg, A.; Bent, S. F. *ACS Catal.* **2015**, *5* (3), 1609−1616.
(31) Miikkulainen, V.; Leskela, M.; Ritala, M.; Puurunen, R. L. *J. Appl. Phys.* **2013**, *113* (2), 021301.
(32) Dasgupta, N. P.; Meng, X.; Elam, J. W.; Martinson, A. B. F. *Acc. Chem. Res.* **2015**, *48* (2), 341−348.
(33) Wang, X.; Gordon, R. G. *ECS J. Solid State Sci. Technol.* **2013**, *2* (3), N41−N44.
(34) Rossnagel, S. M.; Kuan, T. S. *J. Vac. Sci. Technol., B: Microelectron. Process. Phenom.* **2004**, *22* (1), 240−247.
(35) Kumar, N.; Raman, N.; Sundaresan, A. *Z. Anorg. Allg. Chem.* **2014**, *640* (6), 1069−1074.
(36) Gordon, R. G.; Hausmann, D.; Kim, E.; Shepard, J. *Chem. Vap. Deposition* **2003**, *9* (2), 73−78.

DOI: 10.1021/acs.nanolett.5b02508
Nano Lett. XXXX, XXX, XXX−XXX